Relativistic many-body calculation of the electric dipole moment of atomic rubidium due to parity and time-reversal violation

Alok Shukla*
Physics Department, Utah State University, Logan, Utah 84322-4415

B. P. Das*
Clarendon Laboratory, Department of Physics, Oxford University, Oxford OX1 3PU, United Kingdom

J. Andriessen
Radiation and Technology Group, Department of Applied Physics, Delft Univeristy of Technology, Mekelweg 15, 2692 JB, Delft, The Netherlands

(Received 6 August 1993; revised manuscript received 13 January 1994)

In this paper fully *ab initio* calculations of the electric dipole moment (EDM) of atomic rubidium due to two possible mechanisms—the intrinsic electric dipole moment of the electron and the scalar-pseudoscalar coupling between the electrons and the nucleons—are presented. The calculations were carried out using an approach which is a hybrid of the diagrammatic many-body perturbation theory (MBPT) and the multiconfiguration Dirac-Fock method. These calculations, unlike any of the previous MBPT calculations for the rubidium atom, also take into account the effects of electron pair correlations on the atomic EDM. Our results demonstrate that these effects can make significant contributions to the EDM of alkali-metal atoms.

PACS number(s): 31.20.Lr, 31.20.Tz

I. INTRODUCTION

A nonzero electric dipole moment (EDM) of any quantum-mechanical system, in general, and an atom, in particular, will be a signature of nonconservation of parity and time-reversal symmetries [1,2]. The phenomenon of parity nonconservation, ever since its first observation, has been extensively tested in a variety of systems [3]; however, the only evidence of a time-reversal violation, so far, has come indirectly from the *CP*-violating decay of $K^0-\bar{K}^0$ mesons [4]. Therefore, the observation of a nonzero EDM of an atom, besides being direct evidence of T violation, can also throw some light on the mechanisms giving rise to it.

There are several mechanisms that can give rise to the EDM of an atom. Some of them are (i) the intrinsic EDM of an electron, (ii) the intrinsic EDM of nucleons, (iii) P- and T-violating electron-nucleon interactions, (iv) P- and T-violating electron-electron interactions, and (v) P- and T-violating nucleon-nucleon interactions. Any combination of these mechanisms can also give rise to an atomic EDM. However, in this paper we will report the calculations of the EDM of the rubidium atom due to mechanisms (i) and (iii), treating their effects separately. We have considered these effects for atomic rubidium because they are the dominant sources of the EDM of alkali-metal atoms. A brief discussion of the two mechanisms follows.

The Kobayashi-Masakawa mechanism [5], which explains *CP* violation in the standard model of electroweak interactions, predicts an intrinsic EDM of an electron of the order of $10^{-38}e$ cm [6]. However, certain nonstandard models predict it to be about ten to twelve orders of magnitude larger than its standard model value [7]. Various supersymmetric models [8], and models where neutral Higgs boson exchange leads to *CP* violation [9], are of particular importance, as they can lead to the values of the intrinsic EDM of the electron which may be well within the reach of present generation of experiments [10]. If an electron indeed possesses an intrinsic EDM, it will interact with an electric field in much the same way as its magnetic dipole moment interacts with a magnetic field. This interaction can be expressed as an extra term in the field-theoretic Lagrangian of an electron interacting with the electromagnetic field [11]. This extra term gives rise to parity and time-reversal violating terms in the atomic many-body Hamiltonian. In general, these terms correspond to two-body interactions, but the lowest-order term can be reduced to an effective one-body operator [12]. This operator is given by

$$H_{\mathrm{PTV}}^{\mathrm{eff}}=2icd_e\sum_i \beta_i\gamma_{5i}\mathbf{p}_i^2\ , \tag{1}$$

where the subscript PTV refers to the violation of parity and time reversal symmetries, d_e is the intrinsic EDM of the electron, the subscript i runs over the electrons in the

*Present address: Non-Accelerator Particle Physics Group, Indian Institute of Astrophysics, Koramangala, Bangalore 560034, India.

atom, $\mathbf{p}_i$ is the momentum of the ith electron, and β and γ_5 are the Dirac matrices. This term warrants a fully relativistic treatment within Dirac many-body formalism, as any nonrelativistic treatment of this term leads to a zero EDM of the entire atom [13,14]. What one calculates for the atom is the *enhancement factor* [12], which is the ratio of the atomic EDM to that of the electronic EDM,

$$R(\psi)=\frac{(\text{EDM of the atom in state } \psi)}{d_e} . \tag{2}$$

For an alkali-metal atom such as rubidium, the enhancement factor scales as $\sim Z^3\alpha^2$ [12], where Z is the atomic number of the atom and α is the fine-structure constant. This dependence on Z is the reason that experimental searches for an EDM are generally performed on heavy atoms.

A P- and T-violating interaction between electrons and nucleons (protons and neutrons) can arise both from a coupling between scalar and pseudoscalar currents and between tensor currents. The most general short-range neutral current interaction, which does not involve derivative couplings, can be written in the second-quantized form as [15]

$$\mathcal{H}_{\text{PTV}}=\sum_{i=p,n}\left[c_{S(i)}\frac{G_F}{\sqrt{2}}(\bar{N}_i N_i)(\bar{e}i\gamma_5 e)+c_{P(i)}\frac{G_F}{\sqrt{2}}(\bar{N}_i i\gamma_5 N_i)(\bar{e}e)+c_{T(i)}\frac{G_F}{\sqrt{2}}(\bar{N}_i i\gamma_5\sigma_{\mu\nu}N_i)(\bar{e}\sigma^{\mu\nu}e)\right] . \tag{3}$$

$c_{S(i)}$, $c_{P(i)}$, and $c_{T(i)}$ are dimensionless constants which determine the strengths of interactions of, respectively, the scalar, the pseudoscalar, and the tensor currents in the nucleonic sector with appropriate electronic currents, and G_F is the Fermi coupling constant. The symbols N_i and e represent the field operators of nucleons and electrons, respectively. Similar to the case of P and T violation due to an intrinsic electronic EDM, different terms in the P- and T-violating Hamiltonian of Eq. (3) also owe their existence to various models of CP violation in particle physics. Therefore, the study of an atomic EDM due to this interaction can also facilitate a better understanding of the fundamental interactions leading to CP violation in nature. In principle, all the terms of Eq. (3) will contribute to an atomic EDM; however, relative magnitudes of different contributions vary from atom to atom. For paramagnetic atoms such as rubidium, it is the scalar part of the interaction which is the main contributor [15]. Moreover, Barr [16] has shown that in the models where the exchange of neutral Higgs bosons mediates the CP violation (specifically, the two Higgs doublet models), the contribution of the scalar interaction to an atomic EDM can exceed that due to the electronic EDM for certain values of model parameters. However, even though the precision measurements of the EDM of the rubidium atom are underway [17], no theoretical study of this potentially dominant source of its EDM has been conducted before [18]. Therefore, in our calculations we concentrate only on the scalar part of the interaction, and assume $c_{T(i)}=c_{P(i)}=0$. Furthermore, if we use the approximations that the coupling strengths of both the nucleon species are approximately the same

$$c_S=c_{S(n)}\approx c_{S(p)}$$

and that nucleons can be treated nonrelativistically

$$\sum_{i=p,n}(\bar{N}_i N_i)\approx A\rho_N(\mathbf{r}) ,$$

we get the *first-quantized* form of the parity and time-reversal violating interaction

$$H_{\text{PTV}}^{eN}=ic_S\frac{G_F}{\sqrt{2}}A\sum_i\rho_N(\mathbf{r}_i)\beta_i\gamma_{5i} , \tag{4}$$

where $\rho_N(\mathbf{r})$ is the density distribution of the nucleons and A is the total number of nucleons in the isotope under consideration. In our calculations, we have used a Fermi distribution for the nucleon density.

The effect of the P- and T-violating interaction of Eq. (4) for rubidium atom has been evaluated in form of the ratio (we will call it S)

$$S(\psi)=\frac{(\text{EDM of the atom in state } \psi)}{c_S A\dfrac{G_F}{\sqrt{2}}} . \tag{5}$$

The purpose of the present paper is to report a fully *ab initio* calculation for atomic rubidium within the Dirac many-body framework, in which these two CP-violating effects were treated separately and their contributions to the atomic EDM were computed. Though the EDM of atomic rubidium due to the intrinsic EDM of an electron has been evaluated before (see, for example, Refs. [19,20]), to the best of our knowledge this is the first calculation for Rb to take into account a possible P- and T-violating interaction between electrons and nucleons. The method of calculating the EDM is a combination of variational principle and the diagrammatic many-body perturbation theory (MBPT) [21]. The calculations begin at the level of the independent-particle approximation and systematically take into account higher-order effects including pair correlation. We have demonstrated that the contributions of pair correlation to the atomic EDM can be significant; they were found to be approximately 18% of the total atomic EDM for the two cases.

The other purpose behind choosing the Rb atom for our calculations is the following. Theoretical values of the enhancement factor R and the ratio S, in conjunction with the experimental limits on the atomic EDM, can be used to set limits on fundamental quantities d_e and c_S. Therefore, by performing calculations on a variety of systems and comparing them with the corresponding experimental results, one can set independent limits on the *same* fundamental quantities. A comparison among the limits obtained on c_S and d_e from a variety of systems, in our opinion, is the best way to judge the theory as well as the experiments in this field. Our calculations for Rb can be combined with the results of experiments currently underway [17], to get new limits on the values of d_e and c_S.

The paper is organized as follows. In Sec. II we discuss the basics of Dirac many-body theory followed by a description of the theoretical framework outlining our calculations in Sec. III. In Sec. IV we report and discuss the results. In Sec. V we summarize our findings and give an outline for future directions.

II. THEORETICAL BACKGROUND

Here we give a brief review of the mathematical aspects of Dirac many-electron theory, which is the cornerstone of our calculations. We assume that the unperturbed ground state of a many-electron atom is described by the eigenvalue problem

$$H_0|\psi\rangle = E|\psi\rangle \ , \tag{6}$$

where H_0 is the so-called Dirac-Coulomb Hamiltonian for the atomic system

$$H_0 = \sum_i [c\boldsymbol{\alpha}_i \cdot \mathbf{p}_i + \beta_i mc^2 + V_{\rm nuc}(\mathbf{r}_i)] + \sum_{\substack{i,j \\ j<i}} \frac{e^2}{r_{ij}} \tag{7}$$

and $|\psi\rangle$ is, in general, a linear combination of Slater determinants composed of one-electron spinors of the form

$$\phi(\mathbf{r}) = \frac{1}{r} \begin{bmatrix} P(r)\chi_{\kappa m}(\theta,\phi) \\ iQ(r)\chi_{-\kappa m}(\theta,\phi) \end{bmatrix} . \tag{8}$$

These spinors are supposed to be eigenfunctions of angular momentum operators $\mathbf{j}^2$ and $\mathbf{j}_z$, parity operator P, and the operator $K = \beta(\mathbf{1} + \boldsymbol{\sigma} \cdot \mathbf{L})$. In Eq. (8) κ and m refer respectively to the eigenvalues of K and $\mathbf{j}_z$. In addition, the many-electron state $|\psi\rangle$ is also an eigenstate of the total angular momentum and the parity operators.

However, if the parity and time reversal symmetries were being broken by an interaction $H_{\rm PTV}$, then, in the presence of an external electric field E (in the z direction), the total atomic Hamiltonian will be

$$H = H_0 - \sum_i ez_i E + H_{\rm PTV} \ , \tag{9}$$

where $\sum_i ez_i = D$ is the electric dipole operator of the atom. If an atom has a permanent EDM, there will be a shift in its energy when it is exposed to an electric field. If the applied field is sufficiently weak, the shift in the energy will be linear with respect to the field strength. If the change in the energy is W^E, the electric dipole moment of the atom is defined as

$$D = \lim_{E \to 0} \left[-\frac{\partial W^E}{\partial E} \right] . \tag{10}$$

Clearly, the first nonvanishing contribution to the energy shift, which is linear in the strength of the external electric field, is obtained in the second order of the perturbation theory

$$W^E = \sum_{\psi_e \neq \psi} \frac{\langle \psi|H_{\rm PTV}|\psi_e\rangle\langle\psi_e|-\sum_i ez_i E|\psi\rangle}{E_\psi - E_{\psi_e}} + \text{c.c.} \tag{11}$$

Here the E_{ψ_e}'s are the energies corresponding to the intermediate states $|\psi_e\rangle$ and E_ψ is the energy of the state $|\psi\rangle$. Clearly, for W^E to have nonzero value, the parities of the intermediate states $|\psi_e\rangle$ must be opposite that of the unperturbed state $|\psi\rangle$. Using Eq. (10), we get the expression for the EDM of the atom,

$$D = \sum_{\psi_e} \frac{\langle \psi|H_{\rm PTV}|\psi_e\rangle\langle\psi_e|\sum_i ez_i|\psi\rangle}{E_\psi - E_{\psi_e}} + \text{c.c.} \tag{12}$$

In the next section we describe the approach used in calculating the most important terms in the perturbation series of Eq. (12).

III. METHOD OF CALCULATION

The method we have adopted to calculate the EDM of the alkali-metal atoms is a combination of the variational principle and the diagrammatic many-body perturbation theory [21]. In this approach, the expectation value of the EDM is calculated by expressing the atomic wave function in accordance with MBPT, while the unoccupied orbitals needed to compute it are obtained by the multiconfiguration Dirac-Fock (MCDF) method. The computer code implementing the MCDF method used in our calculations used the program by Desclaux [22] to solve the radial difference equations, while employing the MCT and MCP packages of Dyall *et al.* [23] to evaluate various angular coefficients. The method presented here can be applied to all alkali-metal-like atoms. Next, we describe the application of the above-mentioned approach in evaluating the most important MBPT diagrams in the perturbative expansion of an atomic EDM.

A. Independent-particle approximation

The independent-particle approximation is the lowest-order effect giving rise to the atomic EDM. In this approximation, the unperturbed ground state of the atomic system is solved by approximating the effects of electron-electron interaction by means of a central-field potential. Clearly, under the influence of such a potential, electrons move effectively independent of each other, thus justifying the same independent-particle approximation. In our case, we have chosen this central-field potential to be the Dirac-Hartree-Fock potential. The P- and T-violating Hamiltonian $H_{\rm PTV}$ causes the mixing of the independent-particle ground state with configurations of opposite parity, giving rise to a nonzero expectation value of the EDM. The MBPT diagrams which represent this process are shown in Fig. 1. Here v represents the

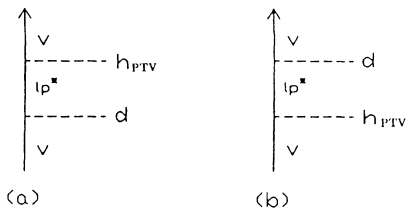

FIG. 1. Lowest-order diagrams.

valence orbital which is 5s for the Rb atom, $|lp^*\rangle$ is an unoccupied $p_{1/2}$ orbital, $h_{\rm PTV}$ is the single-particle P- and T-violating perturbation Hamiltonian, and $d=ez$ is the electric dipole operator corresponding to a single electron. Either the P- and T-violating Hamiltonian $H_{\rm PTV}$ or the dipole operator $\sum_i ez_i$ could be treated as perturbation, and the perturbed wave function could be used to calculate the expectation value of the other operator, to yield the value of the EDM of the atom. However, to make the computations simpler we have treated the dipole operator as the perturbation, i.e.,

$$H_{\rm int}=\sum_i ez_i \ . \tag{13}$$

Clearly, $H_{\rm int}$ can be seen as the perturbation Hamiltonian corresponding to the external electric field of unit strength, acting on the atomic system. With this in mind and using the rules of the diagrammatic MBPT, we get the expression for the diagram in Fig. 1(a) to be

$$D^{(0)}=\sum_l \frac{\langle v|h_{\rm PTV}|lp^*\rangle\langle lp^*|d|v\rangle}{(\varepsilon_v-\varepsilon_{lp^*})} \ , \tag{14}$$

where ε_v, ε_{lp^*}, etc. are the energies associated with the corresponding orbitals. If we define

$$|l'p^*\rangle=\sum_l \frac{|lp^*\rangle\langle lp^*|d|v\rangle}{(\varepsilon_v-\varepsilon_{lp^*})} \ , \tag{15}$$

we get

$$D^{(0)}=\langle v|h_{\rm PTV}|l'p^*\rangle \ . \tag{16}$$

We take the unoccupied orbitals $|lp^*\rangle$ to be the solutions of Dirac-Hartree-Fock (DHF) equation

$$h_0|lp^*\rangle=e_{lp^*}|lp^*\rangle \ ,$$

where h_0 is the single-particle DHF Hamiltonian given by

$$h_0=(c\boldsymbol{\alpha}\cdot\mathbf{p}+\beta mc^2+v_{\rm HF})$$

and $v_{\rm HF}$—the Hartree-Fock potential—is defined by its action on a Hartree-Fock orbital $|i\rangle$,

$$v_{\rm HF}|i\rangle=\sum_{\substack{a\in{\rm core}\\ a\neq i}}\left[\langle a|\frac{1}{r_{12}}|a\rangle|i\rangle-\langle a|\frac{1}{r_{12}}|i\rangle|a\rangle\right] ;$$

then by multiplying Eq. (15) on both the sides by $(h_0-\varepsilon_v)$, we get

$$(h_0-\varepsilon_v)|l'p^*\rangle=-d|v\rangle \ . \tag{17}$$

Therefore if one could solve the differential Eq. (17) to get $|l'p^*\rangle$ and substitute that into Eq. (16), one would get the contribution of the lowest-order MBPT diagram without explicitly performing a sum over the unoccupied states.

We use the MCDF approach to solve for $|l'p^*\rangle$. We assume the atomic wave function to be a linear combination of two configuration states

$$|\psi\rangle=C_1|\phi_0\rangle+C_2|\phi_v^{kp^*}\rangle \ , \tag{18}$$

where $|\phi_0\rangle$ is the Hartree-Fock ground state of the atom and $|\phi_v^{kp^*}\rangle$ is the singly excited configuration state obtained from $|\phi_0\rangle$ by replacing the valence orbital $|v\rangle$ by the unoccupied orbital $|kp^*\rangle$. To solve for $|kp^*\rangle$, we minimize the energy functional with respect to variation in $|kp^*\rangle$, under the orthonormality constraints,

$$\delta_{kp^*}[\langle\psi|H|\psi\rangle-\lambda\langle kp^*|kp^*\rangle-\sum_{k_c}\lambda_{k_c}\langle kp^*|k_cp^*\rangle]=0 \ , \tag{19}$$

where k_c represents occupied orbitals and

$$H=H_0+H_{\rm int} \ , \tag{20}$$

where H_0 and $H_{\rm int}$ were defined in Eqs. (7) and (13), and λ and λ_{k_c} are the Lagrange multipliers that ensure the orthonormality of $|k'p^*\rangle$ with respect to the occupied orbitals of the same symmetry.

It is easy to see that the minimization of the energy functional of Eq. (19) with respect to both the orbital $|kp^*\rangle$ and the configuration coefficients C_1 and C_2 leads to the equation

$$(h_0-\varepsilon_v)\begin{pmatrix}C_2\\ C_1\end{pmatrix}|kp^*\rangle=-d|v\rangle \ , \tag{21}$$

where h_0 is the single-particle DHF Hamiltonian defined earlier and the coefficients C_1 and C_2 are determined by diagonalizing the atomic Hamiltonian in the two-dimensional configuration space spanned by $|\phi_0\rangle$ and $|\phi_v^{kp^*}\rangle$. By comparing Eq. (21) with Eq. (17), we conclude

$$|l'p^*\rangle=\frac{C_2}{C_1}|kp^*\rangle \ . \tag{22}$$

If we substitute this in Eq. (16), we get

$$D^{(0)}=\frac{C_2}{C_1}\langle v|h_{\rm PTV}|kp^*\rangle \ . \tag{23}$$

Therefore, after evaluating all the quantities, we can calculate the contribution of the lowest-order effect represented by the diagram in Fig. 1(a) to the atomic EDM in a straightforward manner by means of Eq. (23). The expression for the diagram in Fig. 1(b) is nothing but the complex conjugate of the one corresponding to the diagram in Fig. 1(a), as both diagrams differ from each other only in the relative time ordering of the $h_{\rm PTV}$ and the d operators. Since the expectation value of a Hermitian operator is a real quantity, the numerical contribution of the complex-conjugated diagram will be the same as that of the original one. Therefore, the total numerical contribution of the two lowest-order diagrams shown in Fig. 1 can be obtained by simply doubling the contribution corresponding to Eq. (23).

B. Core-polarization effects

Here we describe the evaluation of the core-polarization effects in ascending order of perturbation theory.

1. Lowest-order core polarization

Since the outermost shell of an alkali-metal atom is partly filled, a core electron of opposite parity, perturbed by the external field, can get excited and fill the vacancy in the valence shell, thereby leading to a mixed parity atomic state and consequently a nonzero expectation value of the atomic EDM. This is represented by the MBPT diagrams shown in Fig. 2. The expression for the diagram in Fig. 2(a) is

$$D^{(0)}_{\text{c-pol}}=\sum_{k_c}\frac{\langle v|d|k_cp^*\rangle\langle k_cp^*|h_{\text{PTV}}|v\rangle}{\varepsilon_v-\varepsilon_{k_cp^*}}\ , \tag{24}$$

where $|k_cp^*\rangle$ represents a core p^* orbital. The evaluation of this diagram is fairly straightforward as it does not involve the calculation of any unoccupied orbitals. The most important contribution comes from the outermost p^* shell, which is $4p^*$ for rubidium atom. The diagram in Fig. 2(b), which is obtained by the opposite time ordering of the h_{PTV} and the d operators, can be evaluated in an equally straightforward manner.

2. First-order core polarization

Typical first-order core-polarization diagrams are shown in Fig. 3. Here we have one order of perturbation by the Coulomb interaction in addition to the perturbation by the external field.

To illustrate our method of calculation, we will consider the direct diagram shown in Fig. 3(a). The mathematical expression corresponding to the contribution of this diagram to the EDM expectation value is

$$D^{(1)}_{\text{c-pol}}=\sum_l\sum_m\frac{\langle k_cp^*|h_{\text{PTV}}|ms\rangle\langle vms|\frac{1}{r_{12}}|lp^*k_cp^*\rangle\langle lp^*|d|v\rangle}{(\varepsilon_v-\varepsilon_{lp^*})(\varepsilon_{k_cp^*}-\varepsilon_{ms})}\ . \tag{25}$$

We recall the definition Eq. (15), and hence the differential equation satisfied by $|l'p^*\rangle$ will be the same as Eq. (17). With this we get

$$D^{(1)}_{\text{c-pol}}=\sum_m\frac{\langle k_cp^*|h_{\text{PTV}}|ms\rangle\langle vms|\frac{1}{r_{12}}|l'p^*k_cp^*\rangle}{\varepsilon_{k_cp^*}-\varepsilon_{ms}} \tag{26}$$

Now we can define

$$|m's\rangle=\sum_m\frac{|ms\rangle\langle vms|\frac{1}{r_{12}}|l'p^*k_cp^*\rangle}{\varepsilon_{k_cp^*}-\varepsilon_{ms}} \tag{27}$$

so that we eventually get

$$D^{(1)}_{\text{c-pol}}=\langle k_cp^*|h_{\text{PTV}}|m's\rangle\ . \tag{28}$$

From Eq. (27) it is clear that the differential equation satisfied by $|m's\rangle$ is

$$(h_0-\varepsilon_{k_cp^*})|m's\rangle=-|k_cp^*\rangle\langle v|\frac{1}{r_{12}}|l'p^*\rangle\ . \tag{29}$$

If we have already solved for $|l'p^*\rangle$, we can substitute it into Eq. (29) to get a solution for $|m's\rangle$, which in turn can be substituted into Eq. (28) to get the contribution to the EDM expectation value.

To solve for $|l'p^*\rangle$ and $|m's\rangle$, we again use a variational approach. We achieve this by minimizing two different energy functionals with respect to these orbitals. To obtain $|l'p^*\rangle$ we assume the atomic wave function to be

$$|\psi^{(1)}\rangle=C_1|\phi_0\rangle+C_2|\phi_v^{k'p^*}\rangle \tag{30}$$

and minimize the energy functional with respect to variation in $|k'p^*\rangle$, i.e.,

$$\delta_{k'p^*}[\langle\psi^{(1)}|H|\psi^{(1)}\rangle-\lambda\langle k'p^*|k'p^*\rangle-\sum_{k_c}\lambda_{k_c}\langle k_cp^*|k'p^*\rangle]=0\ .$$

Again, k_c runs over the core orbitals only and λ and λ_{k_c} are the Lagrange multipliers imposing orthonormality

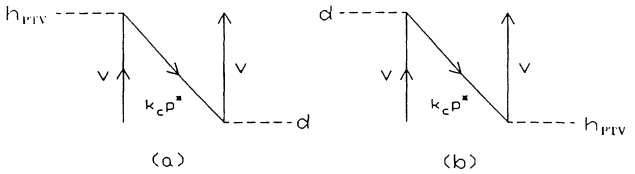

FIG. 2. Lowest-order core-polarization diagrams.

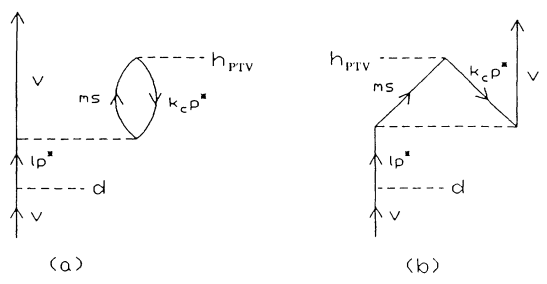

FIG. 3. First-order core-polarization diagrams.

constraint.

The unoccupied orbital $|m's\rangle$ is obtained by assuming the wave function to be

$$|\psi^{(2)}\rangle = C_2|\phi_v^{k'p^*}\rangle + C_3|\phi_{k_cp^*}^{k's}\rangle \ , \tag{31}$$

and varying the energy functional with respect to $|k's\rangle$, i.e.,

$$\delta_{k's}[\langle\psi^{(2)}|H|\psi^{(2)}\rangle - \lambda'\langle k's|k's\rangle - \sum_{m_c}\lambda_{m_c}\langle m_cs|k's\rangle] = 0 \ ,$$

where $|m_cs\rangle$ are the core s orbitals and Lagrange multipliers λ_{m_c} ensure the orthogonality of unoccupied $|k's\rangle$ orbitals to the core s shells. In addition, the two energy functionals above are also minimized with respect to coefficients C_1, C_2, and C_3. This can be achieved by a single diagonalization of the total Hamiltonian in the three-dimensional space spanned by $|\phi_0\rangle$, $|\phi_v^{k'p^*}\rangle$, and $|\phi_{k_cp^*}^{k's}\rangle$; by setting the Hamiltonian matrix elements between $|\phi_0\rangle$ and $|\phi_{k_cp^*}^{k's}\rangle$ to be zero [in agreement with MBPT diagram of Fig. 3(a)]; and by taking the coupling between $|\phi_0\rangle$ and $|\phi_b^{k'p^*}\rangle$ to be weak (as it is mediated by the perturbation $H_{\rm int}$). Under these assumptions the differential equations are found to be

$$(h_0-\varepsilon_v)\frac{C_2}{C_1}|k'p^*\rangle = -d|v\rangle \tag{32}$$

and

$$(h_0-\varepsilon_{k_cp^*})|k's\rangle = -\frac{C_2}{C_3}\langle v|\frac{1}{r_{12}}|k'p^*\rangle|k_cp^*\rangle \ . \tag{33}$$

Therefore, as before, we get

$$|l'p^*\rangle = \frac{C_2}{C_1}|k'p^*\rangle \ .$$

This, when substituted into Eq. (33), gives

$$(h_0-\varepsilon_{k_cp^*})|k's\rangle = -\frac{C_1}{C_3}\langle v|\frac{1}{r_{12}}|l'p^*\rangle|k_cp^*\rangle$$

or

$$(h_0-\varepsilon_{k_cp^*})\frac{C_3}{C_1}|k's\rangle = -\langle v|\frac{1}{r_{12}}|l'p^*\rangle|k_cp^*\rangle \ . \tag{34}$$

By comparing it with Eq. (29), we get

$$|m's\rangle = \frac{C_3}{C_1}|k's\rangle \ , \tag{35}$$

and hence

$$D_{c\text{-pol}}^{(1)} = \frac{C_3}{C_1}\langle k_cp^*|h_{\rm PTV}|k's\rangle \ . \tag{36}$$

Therefore, by substituting the values of various quantities into the expression above, we can evaluate the contribution of the direct core polarization to the value of the atomic EDM. In a similar manner, we can evaluate the exchange core-polarization diagrams.

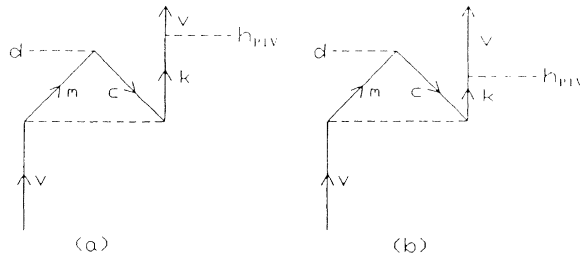

FIG. 4. Core-polarization diagrams which, when added, can be effectively represented by the so-called "pseudodiagram."

3. *The "pseudodiagrams"*

Now we discuss the contributions of the core-polarization diagrams, shown in Fig. 4, to the EDM expectation value. The expressions for the diagrams in Figs. 4(a) and 4(b) are, respectively,

$$D_a = \sum_{k,c,m}\frac{\langle v|h_{\rm PTV}|k\rangle\langle c|d|m\rangle\langle km|\frac{1}{r_{12}}|vc\rangle}{(\varepsilon_v+\varepsilon_c-\varepsilon_k-\varepsilon_m)(\varepsilon_v-\varepsilon_k)} \tag{37}$$

and

$$D_b = \sum_{k,c,m}\frac{\langle v|h_{\rm PTV}|k\rangle\langle c|d|m\rangle\langle km|\frac{1}{r_{12}}|vc\rangle}{(\varepsilon_v+\varepsilon_c-\varepsilon_k-\varepsilon_m)(\varepsilon_c-\varepsilon_m)} \ . \tag{38}$$

By adding Eqs. (37) and (38), we get the total contribution for the two diagrams,

$$D^{(\rm pseudo)} = \sum_{k,c,m}\frac{\langle v|h_{\rm PTV}|k\rangle\langle c|d|m\rangle\langle km|\frac{1}{r_{12}}|vc\rangle}{(\varepsilon_k-\varepsilon_v)(\varepsilon_m-\varepsilon_c)} \ . \tag{39}$$

The mathematical expression shown in Eq. (39) can be represented by the MBPT diagram in Fig. 5. We have called this diagram a "pseudodiagram" because in it the core orbital c is represented by an upward arrow and the unoccupied orbital m is represented by a downward arrow—both contrary to the conventions of the diagram-

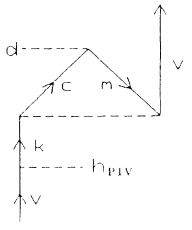

FIG. 5. The pseudodiagram.

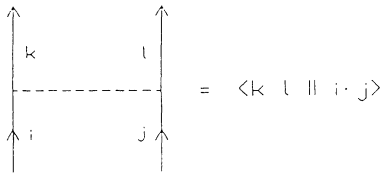

FIG. 6. Antisymmetrized Coulomb vertex used in the pair-correlation diagrams.

matic MBPT. The numerical contributions of the pseudodiagram, and hence those of the two regular diagrams it represents, can be very easily calculated using the computational approach we described in Sec. III B 2. Naturally, such an approach leads to a substantial reduction in the number of MBPT diagrams one needs to evaluate.

C. Pair-correlation effects

Now we turn to the discussion of the calculation of the pair-correlation effects. Here we will use a diagrammatic convention which utilizes the antisymmetrized Coulomb vertices similar to the one illustrated in Fig. 6. Most important contributions of the pair-correlation effects come from what are known as the Brueckner diagrams [24]. These diagrams are shown in the Fig. 7. We will discuss the evaluation of both the lowest-order pair-correlation effects as depicted in Fig. 7(a) and the higher-order pair-correlation effects as shown in Fig. 7(b).

1. Lowest-order pair-correlation effects

Now we will discuss the evaluation of the pair-correlation diagram shown in Fig. 7(a). There are several ways by which one can approach this problem. One of the most frequently used approaches is that of the diagrammatic MBPT using a basis set [25]. According to the rules of the diagrammatic MBPT, the expression for this diagram is

$$D_{\text{pair-cor}}=\sum_{i,j,k,l,c}\frac{\langle v|h_{\text{PTV}}|l\rangle\langle l|d|k\rangle\langle kc||ij\rangle\langle ij||vc\rangle}{(\varepsilon_v-\varepsilon_l)(\varepsilon_v-\varepsilon_k)(\varepsilon_v+\varepsilon_c-\varepsilon_i-\varepsilon_j)} . \tag{40}$$

In this equation the antisymmetrized matrix element is defined as

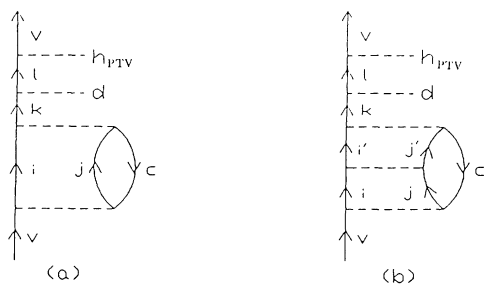

FIG. 7. Brueckner pair-correlation diagrams.

$$\langle ij||kl\rangle=\langle ij|\frac{1}{r_{12}}|kl\rangle-\langle ij|\frac{1}{r_{12}}|lk\rangle .$$

The pair-correlation effects in Eq. (40) can be isolated in the form of a quantity called the *pair function* and defined as

$$\rho_{vc}=\sum_{i,j}\frac{|ij\rangle\langle ij||vc\rangle}{(\varepsilon_v+\varepsilon_c-\varepsilon_i-\varepsilon_j)} . \tag{41}$$

With this Eq. (40) becomes

$$D_{\text{pair-cor}}=\sum_{k,l,c}\frac{\langle v|h_{\text{PTV}}|l\rangle\langle l|d|k\rangle\langle kc||\rho_{vc}\rangle}{(\varepsilon_v-\varepsilon_l)(\varepsilon_v-\varepsilon_k)} . \tag{42}$$

It is possible to calculate the pair function as defined in Eq. (41) explicitly, using a basis set. However, we have adopted a variational-principle-based approach where the pair function is defined as

$$|\rho_{vc}\rangle=\sum_{i,j}C_{(ij)}^{(vc)}|ij\rangle , \tag{43}$$

where $|i\rangle$ and $|j\rangle$ are calculated by the MCDF approach. This is achieved by minimizing the energy functional with respect to the state function

$$|\psi\rangle=C_1|\phi_0\rangle+\sum_{i,j}^{(vc)}C_{(ij)}|\phi_{vc}^{ij}\rangle \tag{44}$$

and the coefficients $C_{(ij)}^{(vc)}$, etc. are obtained by diagonalizing the Hamiltonian in the configuration space spanned by $|\phi_0\rangle$ and $|\phi_{vc}^{ij}\rangle$'s.

Lowest-order pair-correlation effects are evaluated by carrying out the above-mentioned procedure on the wave function

$$|\psi^{(1)}\rangle=C_1|\phi_0\rangle+C_2|\phi_{vc}^{ij}\rangle . \tag{45}$$

The relationship between this variational approach and the perturbative approach described earlier is elaborated in the Appendix.

We can rewrite the Eq. (42) as

$$D_{\text{pair-cor}}=\sum_{l}\frac{\langle v|h_{\text{PTV}}|l\rangle\langle l|d|k^{(*)}\rangle}{\varepsilon_v-\varepsilon_l} , \tag{46}$$

where

$$|k^{(*)}\rangle=\sum_{k,c}\frac{|k\rangle\langle kc||\rho_{vc}\rangle}{\varepsilon_v-\varepsilon_k} . \tag{47}$$

Clearly $|k^{(*)}\rangle$ satisfies the differential equation

$$(\varepsilon_v-h_0)|k^{(*)}\rangle=\sum_{c}\langle c||\rho_{vc}\rangle , \tag{48}$$

where, in general [from Eq. (43)],

$$\langle c||\rho_{vc}\rangle=\sum_{i,j}C_{(ij)}^{(vc)}\left[\langle c|\frac{1}{r_{12}}|i\rangle|j\rangle-\langle c|\frac{1}{r_{12}}|j\rangle|i\rangle\right] . \tag{49}$$

Now Eq. (46) can be written as

$$D_{\text{pair-cor}}=\langle v|h_{\text{PTV}}|l^{(*)}\rangle , \tag{50}$$

where

$$|l^{(*)}\rangle=\sum_l \frac{|l\rangle\langle l|d|\kappa^{(*)}\rangle}{(\varepsilon_v-\varepsilon_l)} \ . \tag{51}$$

It is obvious that $|l^{(*)}\rangle$ satisfies the differential equation

$$(\varepsilon_v-h_0)|l^{(*)}\rangle=d|k^{(*)}\rangle \ . \tag{52}$$

However,we calculate the orbitals $|k^{(*)}\rangle$ and $|l^{(*)}\rangle$ by a variational approach, a brief discussion of which follows.

The orbital $|k^{(*)}\rangle$ is calculated by minimizing the energy functional, i.e.,

$$\delta_{k'}[\langle\psi^{(2)}|H|\psi^{(2)}\rangle-\lambda\langle k'|k'\rangle\sum_{k_c}\lambda_{k_c}\langle k'|k_c\rangle]=0 \ ,$$

where

$$|\psi^{(2)}\rangle=C_2|\phi_{vc}^{ij}\rangle+C_3|\phi_v^{k'}\rangle \tag{53}$$

and k_c stands for the core orbitals of the same symmetry as $|k'\rangle$ orbital. The variation with respect to $|k'\rangle$ leads to the differential equation

$$(\varepsilon_{k'}-h_0)|k'\rangle=\frac{C_2}{C_3}\left\{\langle c|\frac{1}{r_{12}}|i\rangle|j\rangle-\langle c|\frac{1}{r_{12}}|j\rangle|i\rangle\right\} \ , \tag{54}$$

where the energy $\varepsilon_{k'}$ is the DHF energy associated with the unoccupied orbital $|k'\rangle$. From the expression for the variational wave function of Eq. (45) it is clear that the pair function is given by

$$\rho_{vc}=\frac{C_2}{C_1}|ij\rangle \ . \tag{55}$$

Using this, Eq. (54) can be rewritten as

$$(\varepsilon_{k'}-h_0)|k'\rangle=\frac{C_1}{C_3}\langle c||\rho_{vc}\rangle \ .$$

In this equation both the orbital $|k'\rangle$ and the energy $\varepsilon_{k'}$ are unknown parameters and can be solved iteratively. However, if we replace unknown $\varepsilon_{k'}$ by the known parameter ε_v, where ε_v is the DHF ground-state energy of the valence orbital, the differential equation satisfied by $|k'\rangle$ becomes

$$(\varepsilon_v-h_0)\frac{C_3}{C_1}|k'\rangle=\langle c||\rho_{vc}\rangle \ . \tag{56}$$

By comparing Eqs. (56) and (48), we obtain the relationship between the perturbationally and the variationally solved orbitals to be

$$|k^{(*)}\rangle=\frac{C_3}{C_1}|k'\rangle \ . \tag{57}$$

In order to obtain the orbital $|l^{(*)}\rangle$ we assume the atomic wave function to be

$$|\psi^{(3)}\rangle=C_3|\phi_v^{k'}\rangle+C_4|\phi_v^{l'}\rangle \tag{58}$$

and vary the energy functional with respect to the orbital $|l'\rangle$, i.e.,

$$\delta_{l'}[\langle\psi^{(3)}|H|\psi^{(3)}\rangle-\lambda\langle l'|l'\rangle-\sum_{l_c}\lambda_{l_c}\langle l'|l_c\rangle]=0 \ ,$$

where $|l_c\rangle$ represents the core orbitals of the same symmetry as $|l'\rangle$. We get the differential equation satisfied by $|l'\rangle$ to be

$$(\varepsilon_{l'}-h_0)|l'\rangle=\frac{C_3}{C_4}d|k'\rangle \ ,$$

where $\varepsilon_{l'}$ is the unknown energy associated with the orbital $|l'\rangle$. However, as before, we set $\varepsilon_{l'}=\varepsilon_v$ and use Eq. (57) to get

$$(\varepsilon_v-h_0)\frac{C_4}{C_1}|l'\rangle=d|k^{(*)}\rangle \ . \tag{59}$$

Comparing this with Eq. (52) we get

$$|l^{(*)}\rangle=\frac{C_4}{C_1}|l'\rangle \ . \tag{60}$$

By substituting it into Eq. 950) we get the expression for the EDM contribution due to the lowest-order pair-correlation effects to be

$$D_{\text{pair-cor}}=\frac{C_4}{C_1}\langle v|h_{\text{PTV}}|l'\rangle \ . \tag{61}$$

In a pure MCDF calculation, the coefficients C_1, C_2, C_3, and C_4 are determined by diagonalizing the atomic Hamiltonian in the four-dimensional space spanned by $|\phi_0\rangle$, $|\phi_{vc}^{ij}\rangle$, $|\phi_v^{k'}\rangle$, and $|\phi_v^{l'}\rangle$, i.e.,

$$\begin{bmatrix} H_{11} & H_{12} & H_{13} & H_{14} \\ H_{21} & H_{22} & H_{23} & H_{24} \\ H_{31} & H_{32} & H_{33} & H_{34} \\ H_{41} & H_{42} & H_{43} & H_{44} \end{bmatrix}\begin{bmatrix} C_1 \\ C_2 \\ C_3 \\ C_4 \end{bmatrix}=E\begin{bmatrix} C_1 \\ C_2 \\ C_3 \\ C_4 \end{bmatrix} \ , \tag{62}$$

where H_{11}, H_{12}, etc. are defined in Eq. (A3) and

$$\begin{aligned} H_{23}&=\langle\phi_{vc}^{ij}|H|\phi_v^{k'}\rangle \ , \\ H_{33}&=\langle\phi_v^{k'}|H|\phi_v^{k'}\rangle \ , \\ H_{34}&=\langle\phi_v^{k'}|H|\phi_v^{l'}\rangle=\langle k'|d|l'\rangle \ , \\ H_{44}&=\langle\phi_v^{l'}|H|\phi_v^{l'}\rangle \ , \\ &\vdots \ . \end{aligned} \tag{63}$$

But it is clear from Fig. 7 that in the diagrammatic MBPT, unlike MCDF, there is no mixing between the configurations one and three, one and four, and two and four. Since our calculation is based on the diagrammatic MBPT, we set

$$H_{13}=H_{31}=0, \quad H_{14}=H_{41}=0, \quad H_{24}=H_{42}=0 \ ,$$

and the coupling between configurations two and three is considered to be weak, i.e., $H_{23}\approx 0$, again in accordance with the perturbation theory. With this we finally get

$$\begin{bmatrix} H_{11} & H_{12} & 0 & 0 \\ H_{21} & H_{22} & 0 & 0 \\ 0 & 0 & H_{33} & H_{34} \\ 0 & 0 & H_{43} & H_{44} \end{bmatrix} \begin{bmatrix} C_1 \\ C_2 \\ C_3 \\ C_4 \end{bmatrix} = E \begin{bmatrix} C_1 \\ C_2 \\ C_3 \\ C_4 \end{bmatrix} . \quad (64)$$

Therefore, one can solve the Eq. (64) to get all the C coefficients, which in turn can be substituted into Eq. (61) to get the contribution of the pair-correlation diagram to the EDM expectation value.

2. *Higher-order pair-correlation effects*

In our calculations we have calculated up to the second-order pair-correlation effects. A typical diagram representing such effects is shown in Fig. 7(b). Now we will briefly outline the method of evaluation of these diagrams.

The orbital pairs $|i\rangle, |j\rangle$ and $|i'\rangle, |j'\rangle$ are calculated in a self-consistent manner using the MCDF method. Apart from the rules of the angular momentum algebra, there is no restriction on the angular symmetries of these orbitals. But we have restricted ourselves to the diagrams where the orbitals $|i'\rangle, |j'\rangle$ have the same angular momentum values as the orbitals $|i\rangle, |j\rangle$, i.e., they differ from each other only in their principle quantum number n. The reference atomic wave function for the MCDF calculation of these orbitals is taken to be

$$|\psi^{(1)}\rangle = C_1|\phi_0\rangle + C_2|\phi_{vc}^{ij}\rangle + C_3|\phi_{vc}^{i'j'}\rangle . \quad (65)$$

Orbital $|k\rangle$ is calculated by minimizing the energy functional with respect to the wave function

$$|\psi^{(2)}\rangle = C_3|\phi_{vc}^{i'j'}\rangle + C_4|\phi_v^{k'}\rangle ,$$

while the orbital $|l\rangle$ is evaluated by taking the wave function to be

$$|\psi^{(3)}\rangle = C_4|\phi_v^{k'}\rangle + C_5|\phi_v^{l'}\rangle$$

and varying the energy functional with respect to $|l'\rangle$. The differential equations satisfied by the orbitals $|k'\rangle$ and $|l'\rangle$ come out to be identical to the ones in the lowest-order case. By following the same steps, we can show that the expression for the EDM contribution of this diagram is

$$D_{\text{pair-cor}}^{(2)} = \frac{C_5}{C_1}\langle v|h_{\text{PTV}}|l'\rangle . \quad (66)$$

The C coefficients appearing in the expression above are obtained by solving the equations

$$\begin{bmatrix} H_{11} & H_{12} & H_{13} & 0 & 0 \\ H_{21} & H_{22} & H_{23} & 0 & 0 \\ H_{31} & H_{32} & H_{33} & 0 & 0 \\ 0 & 0 & 0 & H_{44} & H_{45} \\ 0 & 0 & 0 & H_{54} & H_{55} \end{bmatrix} \begin{bmatrix} C_1 \\ C_2 \\ C_3 \\ C_4 \\ C_5 \end{bmatrix} = E \begin{bmatrix} C_1 \\ C_2 \\ C_3 \\ C_4 \\ C_5 \end{bmatrix} , \quad (67)$$

where

$$\begin{aligned} H_{23} &= \langle \phi_{vc}^{ij}|H|\phi_{vc}^{i'j'}\rangle , \\ H_{33} &= \langle \phi_{vc}^{i'j'}|H|\phi_{vc}^{i'j'}\rangle , \\ &\vdots \\ H_{45} &= \langle \phi_v^{k'}|H|\phi_v^{l'}\rangle = \langle k'|d|l'\rangle , \\ H_{55} &= \langle \phi_v^{l'}|H|\phi_v^{l'}\rangle , \\ &\vdots \end{aligned} \quad (68)$$

IV. RESULTS AND DISCUSSIONS

In this section we report and discuss the results of our calculations of the electric dipole moment of the atomic rubidium. We also compare our results for the rubidium EDM, due to the intrinsic EDM of the electron, with other published calculations. However, for the case of the rubidium EDM due to P- and T-violating interaction between the electrons and the nucleons, such a comparison is not possible because of the lack of any prior calculations. All the numerical values that we are reporting are expressed in the atomic units. In what follows we systematically describe our results in the order of importance of the MBPT diagrams they represent.

A. Lowest-order effect

This effect, which is represented by the MBPT diagrams shown in Fig. 1, is the most important in terms of its contribution to the total electric dipole moment of the rubidium atom. As is clear from these diagrams, this effect arises due to direct interaction between the valence electron ($v = 5s$) of the rubidium atom and either the P- and T-violating Hamiltonian h_{PTV} or the external field Hamiltonian d. As a result of this interaction, the valence electron, which is bound very weakly to the atom, is now described by a mixed-parity single-particle state (in this case a mixture of $5s$ and lp^* orbitals). This implies that the atom—no longer in a definite parity state—will have a nonvanishing expectation value of the electric dipole moment. The results we obtained for these lowest-order calculations for the ground state of the rubidium atom are as follows. The value of the enhancement factor R, which is the ratio of the atomic EDM to that of a single electron, was evaluated to be

$$R^{(0)} = 19.8087 .$$

The value above is within 2% of the results of a prior calculation by Das, Johnson, and Idrees [26]. For the case of the EDM due to a P- and T-violating electron-nucleon interaction, the S ratio, which is defined as the ratio of the total atomic EDM to the scalar-pseudoscalar coupling constant c_S, was found to be

$$S^{(0)} = 12.2568 .$$

B. Core-polarization effects

In what follows, we will discuss various mechanisms which lead to core-polarization effects and also their numerical contributions.

TABLE I. Contributions of the lowest-order core-polarization MBPT diagrams shown in Fig. 2.

Core orbital k_cp^*	Enhancement factor R	S ratio
$4p^*$	0.9434	0.5838
$3p^*$	0.009	0.0056
Total	0.9524	0.5894

1. Lowest-order core polarization

The valence shell $5s$ for the rubidium atom in its Dirac-Fock ground state is not a completely filled shell. Therefore, an electron from one of the core p^* orbitals, by interacting with either the parity and time-reversal Hamiltonian or the external field, can get excited into the valence shell, thus contributing to the atomic EDM. The MBPT diagrams which depict these processes for a general core p^* orbital k_cp^* are shown in Fig. 2. The results of these calculations are described in Table I. It is clear from the results that the largest contribution to this set of diagrams, as expected, comes from the one involving the excitation of $4p^*$ orbital. The contribution of the next diagram, in which $3p^*$ orbital is excited, is two orders of magnitude smaller than the largest one. This clearly demonstrates the rapid convergence of the calculations for this set of diagrams.

2. First-order core polarization

These effects are different from the lowest-order core polarization in that in addition to h_{PTV} and d, one order of Coulomb interaction is also involved in the process. Now we will describe various types of diagrams which come under this category.

(a) EDM core-polarization effects. Various MBPT diagrams that represent this effect are shown in Fig. 8. For example, if we look at the diagram in Fig. 8(e), it is clear that a core electron (labeled c) is excited into an unoccupied orbital (labeled m) of opposite parity by means of its interaction with h_{PTV}. Next, the electron in the orbital m interacts with the valence electron by means of Coulomb interaction resulting in the deexcitation of the valence electron into the core shell c and transition of the electron in the orbital m to the orbital kp^*. This kp^* orbital is the same as the one in the lowest-order case. Finally, the electron in the orbital kp^* is deexcited into the valence shell because of its interaction with the external field Hamiltonian d. Since in these processes a core electron is excited into an unoccupied orbital of opposite parity by means of its interaction with h_{PTV} (the EDM causing perturbation Hamiltonian), these diagrams are referred to as the EDM core-polarization diagrams. In general, all the diagrams shown in Fig. 8 are supposed to contribute to the atomic EDM, but for the special case of the EDM core-polarization diagrams, the contribution of the direct diagrams (both regular and pseudo) is identically zero [27].

(b) External-field core polarization. The diagrams representing this effect are shown in Fig. 9. As is clear from the diagrams, here the core electron (labeled c) is excited into an unoccupied orbital (labeled m) of opposite parity by means of its interaction with the external field Hamiltonian d, thus justifying the name *external-field core polarization.* Including the contributions of this type of diagrams amounts to including the effects of EDM shielding due to the presence of an external field. This is manifested in the numerical results in that the contribution of this class of diagrams is opposite in sign compared to the contribution of the EDM core-polarization diagrams. Since the dipole operator d is a vector operator, it can connect states of opposite parities which satisfy the angular momentum selection rule $\Delta j=0,1$. When we compare this to the case of EDM core polarization, where the corresponding selection rule was $\Delta j=0$ owing to the fact that h_{PTV} is a scalar operator, it becomes obvious that for the case of the external-field core polarization, there are more possible values of m and c. In addition to this, unlike EDM core-polarization diagrams, direct external field core-polarization diagrams shown in Figs. 9(a)—9(d), in general, have nonvanishing contributions. Therefore, the number of the MBPT diagrams that contribute to external-field core polarization is more compared to the ones which contribute to the EDM core polarization.

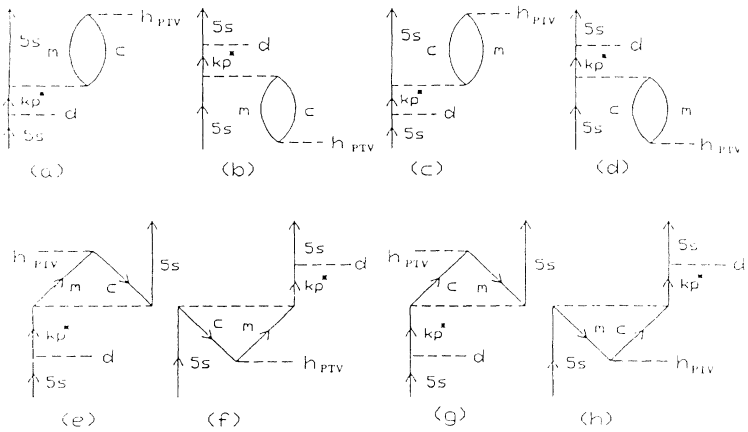

FIG. 8. EDM core-polarization diagrams.

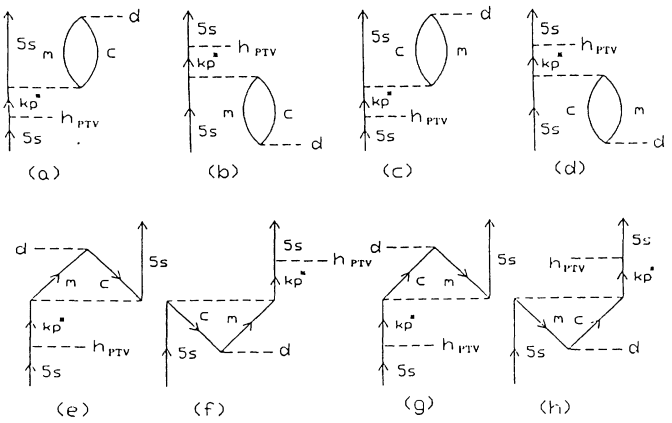

FIG. 9. External-field core-polarization diagrams.

3. *Core-polarization effects: Results and comparison*

The final contributions of different types of core-polarization effects to the electric dipole moment of the rubidium atom are presented in Table II. Now we will compare our lowest-order and core-polarization results with other similar calculations. Johnson *et al.* in their two papers [19,20] have presented the results of their calculations of the enhancement factor R of the rubidium atom. The first of these papers [19] presents the results of their "lowest-order" calculations. The philosophy behind their approach is similar to the one behind our lowest-order calculations in that they assume that the main contribution to the atomic EDM comes from the perturbation caused to the valence orbital due to $h_{\rm PTV}$. They assume the perturbed valence orbital $|v'\rangle$ to be

$$|v'\rangle = |v\rangle + |w\rangle \ .$$

Here $|v\rangle$ is the unperturbed valence orbital ($5s$ for Rb) and $|w\rangle$ is perturbation correction, of opposite parity, caused by its interaction with $h_{\rm PTV}$. The differential equation, sometimes referred to in the literature as the parity-nonconserving-Hartree-Fock (PNC-HF) equation [27], which $|w\rangle$ satisfies is

$$(h_0 - \varepsilon_v)|w\rangle = -h_{\rm PTV}|v\rangle - v_{\rm HF}^{(1)}|v\rangle \ , \tag{69}$$

where h_0 is the single-particle Hartree-Fock Hamiltonian, ε_v is the orbital energy of the valence orbital $|v\rangle$, and $v_{\rm HF}^{(1)}$ is the first-order (in $h_{\rm PTV}$) correction to the Hartree-Fock potential which takes into account the effects of $h_{\rm PTV}$ on the core orbitals. The corrections included in $v_{\rm HF}^{(1)}$ are shown diagrammatically in Fig. 10. From these diagrams and Eq. (69) it is clear that the lowest-order results of Johnson *et al.* contain EDM core-polarization effects which include certain terms to all orders in Coulomb interaction. In their second paper [20], they go beyond their lowest-order calculations by doing MBPT calculations which include the external field core-polarization effects to the first order in the Coulomb interaction with an external field vertex (i.e., d vertex) modified in accordance with the random-phase approximation (RPA). Using an RPA-modified vertex results in the inclusion of some terms of second- and higher-order perturbation theory in the Coulomb interaction.

This is to be contrasted with our approach, where the lowest-order calculations are carried out by evaluating the perturbation correction to the valence orbital, by solving the differential equation

$$(h_0 - \varepsilon_v)|w\rangle = -h_{\rm PTV}|v\rangle \ . \tag{70}$$

A comparison between Eqs. (69) and (70) tells us that our lowest-order result, unlike that of Johnson *et al.*, does not include the EDM core-polarization effects. In our calculations, EDM core polarization and external-field core polarization are treated on equal footing in that both these effects are evaluated as perturbations beyond the lowest-order calculations, including the effects of Coulomb interaction only to the first order. Keeping these differences in mind, it is valid to compare the lowest-order results of Johnson *et al.*, with our *lowest-order + EDM core-polarization* results. The final results of Johnson *et al.* [20] will be compared with our *lowest order + EDM core-polarization + external-field core-polarization* results. In addition to this, we also mention the results of the calculations by Sandars [28]. Since these calculations were carried out using a local-potential

TABLE II. Final contributions of both types of core-polarization effects to the EDM of the Rb atom.

Type of effect	Enhancement factor R	S ratio
Lowest-order core polarization	0.9524	0.5894
EDM core polarization	2.3847	1.4392
External-field core polarization	−1.2537	−0.7758
Total	2.0834	1.2528

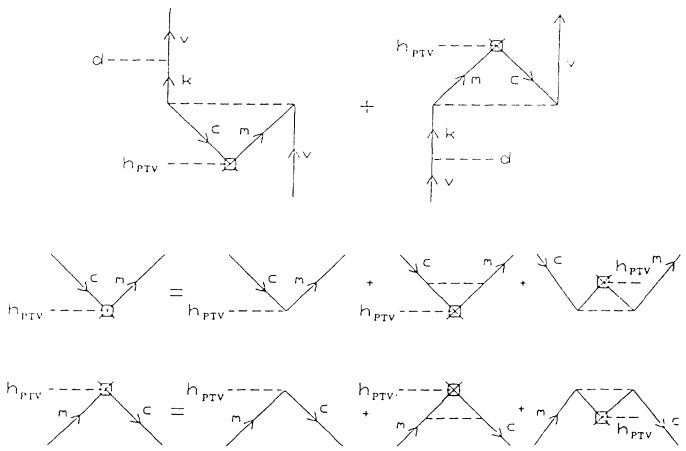

FIG. 10. First row of diagrams defines the terms in perturbation theory corresponding to $v_{\mathrm{HF}}^{(1)}$. Subsequent rows define the dressed vertex occurring in the first row [19].

based approach, it is difficult to make an exact comparison with our results. However, a rough correspondence can be established by recognizing that the "shielded" results in these calculations were arrived at by taking into account the effects of the polarizability of the atomic core (under the influence of the external field), unlike the "unshielded" case. The results of our calculations are presented alongside those of the calculations mentioned above in Tables III–V. The difference between the results can probably be explained by the fact that our calculations of the EDM core-polarization effects are only to the first order in the Coulomb interaction, while those of Johnson *et al.* contain certain effects that include the Coulomb interaction to all orders in perturbation theory. But still, at every stage, the two results are within 15% of each other. We describe the effects of pair correlation in the next section.

C. Pair-correlation effects

The ground-state wave function of the rubidium atom that we have used in our calculations is calculated under the Hartree-Fock approximation, which is a central-field approximation and takes into account the effects of electron-electron interactions only in an average manner. In order to account for this shortcoming of the atomic ground state, and to see as to how the inclusion of the electron correlation effects affects the value of the atomic EDM, one should evaluate what are called the *pair-correlation diagrams.* Various types of MBPT diagrams representing the pair-correlation effects are shown in Figs. 11 and 12. In the diagrammatic language, these diagrams take into account the effects of excitation of two electrons simultaneously from the Hartree-Fock ground state, under the influence of mutual Coulomb repulsion. In principle, these two electrons could be any two electrons belonging to the ground state of the atom, but it is clear that the most important effects for alkali-metal atoms will involve a valence-core correlation, i.e., when one of the excited electrons is the valence electron. The pair-correlation effects not only provide important contributions to the unperturbed ground state but also to the ground state already perturbed by the h_{PTV} or d operators. Such effects are represented, for example, by the diagrams shown in Figs. 11(e), 11(f), 12(e), and 12(f). In the preceding sections, all the cases we discussed involved the single excitations, i.e., at one point only one electron (core or valence) had been excited from the ground state. Therefore, while doing the pair-correlation calculations, we have evaluated the terms in the perturbation series which correspond to the simultaneous excitation of both the core and the valence electrons. We call the diagrams that contain two orders of Coulomb interaction, shown in Fig. 11, the *lowest-order pair-correlation diagrams.* The diagrams that contain three orders (or more) of Coulomb interactions as shown in Fig. 12 will be referred to as the *higher-order pair-correlation diagrams.* As we shall see, the main contribution to the pair-correlation effects comes from the lowest-order diagrams. But we have evaluated selected higher-order diagrams to demonstrate the completeness and the convergence of our calculations. Now we will describe our results for both types of diagrams.

1. Lowest-order pair-correlation effects

If we consider a typical lowest-order pair-correlation diagram, for example, the one in Fig. 11(a), it is clear that

TABLE III. Comparison between our calculations inclusive of the EDM core-polarization effects and the calculations of Johnson *et al.* [19] and Sandars [28] for the enhancement factor R.

Our calculations	Other calculations	
Lowest order + EDM core polarization	PNC-HF [19]	Unshielded [28]
23.1	26.6	27.5

TABLE IV. Comparison between our results of the external-field core-polarization corrections to R and the similar calculations of Johnson *et al.* [20].

Our calculations	Other calculations [20]
−1.2	−2.0

one of the core electrons (labeled c) interacts with the valence electron ($5s$) via Coulomb interaction resulting in the excitation of both the electrons to unoccupied shells labeled i and j. In mathematical terms, this amounts to nothing but adding a doubly excited (relative to the Hartree-Fock state) configuration state function to the Hartree-Fock ground-state wave function, as discussed in Sec. III C 1. These two electrons interact again via the Coulomb interaction leading to the deexcitation of one of the electrons back to the core shell c while the other electron makes a transition to another unoccupied s shell labeled ls. Beyond this, the action of h_{PTV} and d vertices is similar to the one in the lowest-order case discussed in Sec. III A. We expect to see the trend that the most important contributions to this effect should come from the diagrams which involve the excitation of the outermost core electrons, with the contribution decreasing successively as one goes deeper in the core. Different core-valence pairs were considered in our calculations. Corresponding results for various diagrams are presented in Tables VI–VIII. The total first-order pair-correlation contributions are listed in Table IX.

2. *Higher-order pair-correlation effects*

In principle, one could evaluate the pair-correlation effects up to any order in Coulomb interaction, but we will confine our discussion to the higher-order effects that are third order in Coulomb interaction. As we shall see, the contribution of these terms comes out to be only a fraction of the contribution of the lowest-order terms, thus justifying the neglect of the higher-order terms. These terms are shown in the diagrammatic form in Fig. 12. It is clear from these diagrams that these effects arise when the pair of electrons which interact with each other to give rise to the lowest-order effects interacts once more via the mutual Coulomb interaction. In mathematical terms this amounts to adding another doubly excited configuration state to the ground state already perturbed

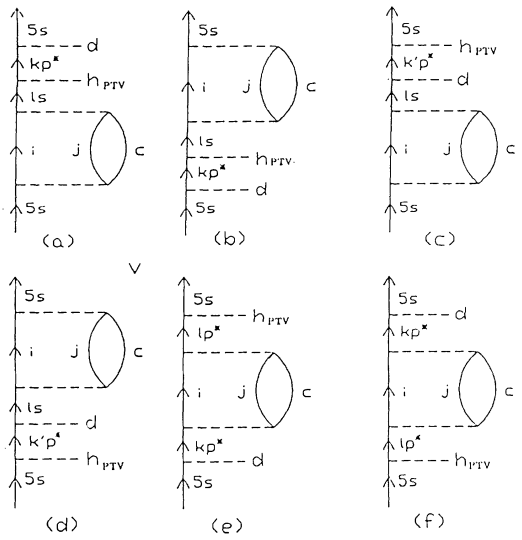

FIG. 11. Lowest-order pair-correlation diagrams.

by the lowest-order effect. In principle, the second pair of orbitals i' and j' can be of any angular symmetry consistent with the angular momentum selection rules. In our calculations, however, we have evaluated only those diagrams in which the angular symmetries of i' and j' are same as those of i and j, i.e., i' and j' differ from i and j only in the principle quantum number. We have evaluated the higher-order diagrams corresponding to only those lowest-order diagrams whose contributions were significant. Corresponding results for various diagrams are presented in Tables X—XIII.

3. *Pair correlation: Final results*

The final results of our calculations of the contributions of the pair-correlation effects to the electric dipole moment of the atomic rubidium are presented in Tables XIV and XV. Table XIV lists these contributions classified according to the orders of pair correlation and also the core orbitals that were involved in the process. Table XV shows the total contributions to the atomic electric dipole moments which arise from different orders of pair correlation.

The trend that is quite evident in these tables is that at the level of every order of electron correlation (as it was at the level of the individual diagrams also), the diagrams

TABLE V. Comparison between our results inclusive of both the EDM and the external-field-induced core-polarization effects and the calculations of Johnson *et al.* [20] and Sandars [28] for the enhancement factor R.

Our calculations	Other calculations	
Lowest order +EDM core polarization +external-field core polarization	PNC-HF +external field core polarization [20]	Shielded [28]
21.9	24.6	24

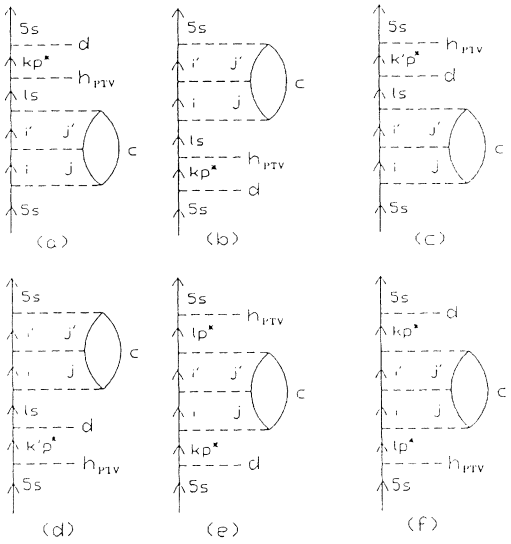

FIG. 12. Higher-order pair-correlation diagrams.

which involve $4p$ orbital in the pair-correlation process contribute the most, followed by those involving $4p^*$. The contribution of the diagrams involving $4s$ orbital is extremely small and insignificant compared to the other two. This trend can be easily understood if we consider the fact that of the three orbitals $4p$ is the least tightly bound to the nucleus while $4s$ is the most. Therefore, an electron in the $4p$ orbital is most easily excitable to an unoccupied orbital because of the pair-correlation process (which involves Coulomb repulsion) with another electron (valence or excited), as compared to the electrons in the other two shells, thus explaining the highest contribution of the $4p$ electrons. The fact that the contribution of the $4s$ electron is so much smaller (only a fraction of a percent of the total contribution), we are confident that our calculations, which take into account the effects of valence-core correlation, are essentially complete and that we do not need to go any further into the core.

The other result that is quite obvious is that the total contribution of the higher-order pair-correlation diagrams is only a small fraction of their lowest-order counterparts. From this we conclude that the most important contributions to the atomic EDM due to pair-correlation effects arise from the lowest-order diagrams and that the contributions will decrease rapidly as we go to the higher

TABLE VI. Total contributions of the pair-correlation diagrams of the type shown in Figs. 11(a) and 11(b), classified according to the core orbital c.

Core orbital c	Enhancement factor R	S ratio
$4p$	1.6636	1.0294
$4p^*$	0.8391	0.5192
$4s$	0.0298	0.0185
Total	2.5325	1.5671

TABLE VII. Total contributions of the pair-correlation diagrams of the type shown in Figs. 11(c) and 11(d). Results are classified according to the core orbital that was involved in the pair-correlation process.

Core orbital c	Enhancement factor R	S ratio
$4p$	−0.5027	−0.311
$4p^*$	−0.3466	−0.2145
$4s$	−0.0023	−0.0014
Total	−0.8516	−0.5269

TABLE VIII. Total contributions of the pair-correlation diagrams of the type shown in Figs. 11(e) and 11(f), classified according to the core orbital.

Core orbital c	Enhancement factor R	S ratio
$4p$	1.6257	1.0058
$4p^*$	1.0321	0.6386
$4s$	0.0092	0.0057
Total	2.667	1.6501

TABLE IX. Total contributions of the lowest-order pair-correlation diagrams of the type shown in Fig. 11, classified according to the core orbitals.

Core orbital c	Enhancement factor R	S ratio
$4p$	2.7866	1.7242
$4p^*$	1.5246	0.9433
$4s$	0.0367	0.0228
Total	4.3479	2.6903

TABLE X. Total contributions of the pair-correlation diagrams of the type shown in Figs. 12(a) and 12(b), classified according to the core orbital.

Core orbital c	Enhancement factor R	S ratio
$4p$	0.2608	0.1614
$4p^*$	0.0799	0.0494
Total	0.3407	0.2108

TABLE XI. Total contributions of the pair-correlation diagrams of the type shown in Figs. 12(c) and 12(d), classified according to the core orbital.

Core orbital c	Enhancement factor R	S ratio
$4p$	−0.035	−0.0217
$4p^*$	−0.0128	−0.0079
Total	−0.0478	−0.0296

TABLE XII. Total contributions of the pair-correlation diagrams of the type shown in Figs. 12(e) and 12(f), classified according to the core orbital.

Core orbital c	Enhancement factor R	S ratio
$4p$	0.1164	0.0721
$4p^*$	0.0275	0.0177
Total	0.1439	0.0898

TABLE XIII. Total contributions of the higher-order pair-correlation diagrams of the type shown in Fig. 12, classified according to the core orbital.

Core orbital c	Enhancement factor R	S ratio
$4p$	0.3422	0.2118
$4p^*$	0.0946	0.0592
Total	0.4368	0.271

orders in Coulomb interaction. This clearly demonstrates the rapid convergence of the perturbation series as far as this type of pair-correlation effect is concerned.

V. SUMMARY

In Table XVI we summarize our calculations of the electric dipole moment of atomic rubidium both due to the intrinsic electric dipole moment of the electron and the P- and T-violating interaction between the electrons and the nucleons. It is quite clear from the results that the contribution of the pair correlation to the electric dipole moment of atomic rubidium can be quite significant. Though, our calculations probably underestimate the core-polarization effects; however, results suggest that pair-correlation effects can be as significant as core polarization. In what follows we describe some of the limitations of our calculations which could possibly be overcome by further efforts in the future.

As we have mentioned before, one of the major limitations of our calculations is that we have taken into account the effects of core polarization only to the first order in the Coulomb interaction. One could, in principle, account for these effects to all orders in Coulomb interaction using either a differential-equation-based approach or an MBPT-oriented approach using dressed vertices for the d operator or h_{PTV} [19,20].

In the pair-correlation calculations, our correlation orbitals i and j, though calculated in a self-consistent manner with each other, are not calculated self-consistently with the occupied orbitals of the atom. We solve for orbitals i and j using the unperturbed ground-state (i.e., Hartree-Fock state) solutions of the core and

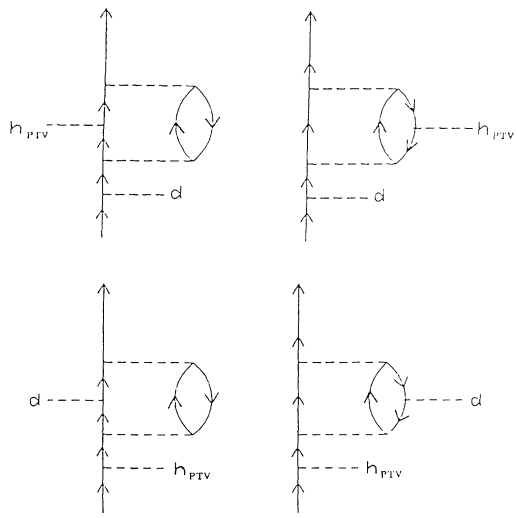

FIG. 13. Some of the pair-correlation diagrams that were not included in the calculations.

valence orbitals. However, we did check our solutions of orbitals i and j for a given diagram for orthogonality with other (both occupied and unoccupied) orbitals of the same symmetry. Similarly, correlation orbitals of the same angular symmetry, but calculated for different diagrams, are quite different from each other. This is due to the fact that the correlation orbitals are calculated by means of an MCDF calculation (see Sec. III C 1), which is unique to every diagram. This feature of our calculations makes them different from the diagrammatic MBPT calculations done using a basis set where the same set of orbitals are used in different calculations. In our pair-correlation calculations, we have taken into account only those diagrams which involve core-valence correlation; i.e., we have completely ignored the core-core correlation effects. It is our belief that these effects will be small because most of the contribution to the atomic EDM comes from the diagrams where the valence electron is perturbed. But, for the sake of completeness, one may wish to verify this by means of actual calculations. Also ig-

TABLE XIV. Total contributions of all the pair-correlation diagrams combined, classified in accordance with the core orbital and the order of correlation. The dash denotes a contribution not evaluated.

Core orbital c	Order of correlation	Enhancement factor R	S ratio
$4p$	Lowest	2.7866	1.7242
	Higher	0.3422	0.2118
$4p^*$	Lowest	1.5246	0.9433
	Higher	0.0946	0.0592
$4s$	Lowest	0.0367	0.0228
	Higher	—	—
Total		4.7847	2.9613

TABLE XV. Total contributions of all the pair-correlation diagrams combined, classified according to the order of correlation.

Order of correlation	Enhancement factor R	S ratio
Lowest	4.3479	2.6903
Higher	0.4368	0.271
Total	4.7847	2.9613

nored in our calculations were the diagrams which do not belong to the category of Brueckner pair-correlation diagrams. Some of these diagrams are shown in Fig. 13. Some of these diagrams could also provide important contributions to the atomic electric dipole moment. Bearing in mind all the limitations of our calculations mentioned above, we do not intend to present our results as the last word on the evaluation of the EDM of the rubidium atom. However, we do believe that our calculations have demonstrated that the contribution of the pair-correlation effects to the atomic EDM can be significant and therefore should not be ignored.

The above discussion exposes one of the largest weaknesses of the diagrammatic MBPT—the large number of diagrams one has to evaluate to bring the calculations anywhere near complete as far as a given order of the perturbation theory is concerned. And to make matters worse, the number of possible diagrams proliferates tremendously as one goes to higher order in perturbation theory. However, there is an alternative nonperturbative approach to many-electron systems which shares the desirable property of "size extensivity" with MBPT, but with a much simpler diagrammatic "bookkeeping." This approach is called the coupled-cluster approach [29], and in future publications [30] we intend to pursue its implementation to the problem of the electric dipole moment of alkali-metal-type atoms.

APPENDIX: LOWEST-ORDER PAIR CORRELATION: RELATIONSHIP BETWEEN THE PERTURBATION AND THE VARIATIONAL APPROACHES

Lowest-order pair-correlation effects are evaluated by working in a two-dimensional configuration space. Now we will examine the connection between our variational approach and the perturbation approach we outlined in Sec. III C 1. The atomic state function used in our calculation is of the form

TABLE XVI. Final contributions of various effects to the EDM of the Rb atom.

Type of effect	Enhancement factor R	S ratio
Lowest order	19.8087	12.2568
Core polarization	2.0834	1.2528
Pair correlation	4.7847	2.9613
Total	25.6768	16.4709

$$|\psi^{(1)}\rangle = C_1|\phi_0\rangle + C_2|\phi_{vc}^{ij}\rangle \ , \tag{A1}$$

where $|i\rangle$ and $|j\rangle$ are unoccupied orbitals which are evaluated by the MCDF method. Minimizing the energy functional with respect to the coefficients C_1 and C_2 amounts to diagonalizing the atomic Hamiltonian in the two-dimensional space spanned by $|\phi_0\rangle$ and $|\phi_{vc}^{ij}\rangle$ and leads to the condition

$$\begin{bmatrix} H_{11} & H_{12} \\ H_{21} & H_{22} \end{bmatrix} \begin{bmatrix} C_1 \\ C_2 \end{bmatrix} = E \begin{bmatrix} C_1 \\ C_2 \end{bmatrix} , \tag{A2}$$

where

$$\begin{aligned} H_{11} &= \langle \phi_0|H|\phi_0\rangle \ , \\ H_{12} &= \langle \phi_0|H|\phi_{vc}^{ij}\rangle = \langle vc\|ij\rangle \ , \\ H_{21} &= \langle \phi_{vc}^{ij}|H|\phi_0\rangle = \langle ij\|vc\rangle \ , \\ H_{22} &= \langle \phi_{vc}^{ij}|H|\phi_{vc}^{ij}\rangle \ . \end{aligned} \tag{A3}$$

We can solve Eq. (A2) to get

$$\frac{C_2}{C_1} = -\frac{(H_{11}-H_{22})}{2H_{12}} \pm \frac{(H_{11}-H_{22})}{2H_{12}} \left[1+\frac{4|H_{12}|^2}{(H_{11}-H_{22})^2}\right]^{1/2} . \tag{A4}$$

If the coupling between the configurations is not too strong (which is what is assumed in a perturbation treatment of correlation), i.e.,

$$|H_{12}|^2 \ll (H_{11}-H_{22})^2 \ , \tag{A5}$$

we can binomially expand the right-hand side of Eq. (A4) to get

$$\frac{C_2}{C_1} = -\frac{(H_{11}-H_{22})}{2H_{12}} \pm \frac{(H_{11}-H_{22})}{2H_{12}} \left\{1+\frac{2|H_{12}|^2}{(H_{11}-H_{22})^2}\right\} .$$

The solution consistent with the weak coupling will be

$$\frac{C_2}{C_1} = \frac{|H_{12}|}{(H_{11}-H_{22})} + (\text{higher-order terms in } H_{12}) \ . \tag{A6}$$

If we assume the intermediate normalization for the wave function $|\psi\rangle$, and substitute this in Eq. (A1), we get

$$|\psi\rangle = |\phi_0\rangle + \frac{|H_{12}|}{(H_{11}-H_{22})}|\phi_{vc}^{ij}\rangle + (\text{higher-order terms in } H_{12}) \ .$$

However, we know that

$$H_{11}-H_{22} = \langle \phi_0|H|\phi_0\rangle - \langle \phi_{vc}^{ij}|H|\phi_{vc}^{ij}\rangle \ .$$

If we make the crude approximation [31],

$$H_{11}-H_{22} \approx \varepsilon_c + \varepsilon_v - \varepsilon_i - \varepsilon_j \ ,$$

and use Eq. (A3), we get above

$$|\psi\rangle \approx |\phi_0\rangle + \frac{\langle ij \| vc \rangle}{\varepsilon_v + \varepsilon_c - \varepsilon_i - \varepsilon_j} |\phi_{vc}^{ij}\rangle + (\text{higher-order terms in } H_{12}) \, . \quad \text{(A7)}$$

If we compare Eq. (A7) with Eq. (41), we begin to see similarities between the variational wave function and the perturbation wave function in the first order of electron correlation. But, as is obvious above, the variational wave function, unlike its perturbation counterpart, also contains higher-order terms in the electron correlation.

[1] T. D. Lee and C. N. Yang, Brookhaven National Laboratory Report No. BNL 443-T91, 1957 (unpublished).

[2] L. D. Landau, Nucl. Phys. **3**, 127 (1957).

[3] For a review see E. N. Fortson and L. L. Lewis, Phys. Rep. **113**, 289 (1984).

[4] J. R. Christensen, J. W. Cronin, V. L. Fitch, and R. Turlay, Phys. Rev. Lett. **13**, 138 (1964).

[5] M. Kobayashi and T. Maskawa, Prog. Theor. Phys. **49**, 652 (1973).

[6] F. Hoogeven, Nucl. Phys. **B341**, 322 (1990).

[7] See the following: B. W. Lynn, in *Atomic Physics 9*, edited by R. S. Van Dyck, Jr. and E. N. Fortson (World Scientific, Singapore, 1984); S. M. Barr and W. J. Marciano, in *CP Violation*, edited by C. Jarlskog (World Scientific, Singapore, 1989); W. Bernreuther and M. Suzuki, Rev. Mod. Phys. **63**, 313 (1991).

[8] W. Fischler, S. Paban, and S. Thomas, Phys. Lett. B **289**, 373 (1992); also see Ref. [7].

[9] For the models leading to *CP* violation by Higgs boson exchange see S. Weinberg, Phys. Rev. Lett. **63**, 2339 (1989); Phys. Rev. D **42**, 860 (1990). For implications of these models to electronic EDM see S. M. Barr and A. Zee, Phys. Rev. Lett. **65**, 21 (1990); J. Gunion and R. Vega, Phys. Lett. B **251**, 157 (1990); D. Chang, W.-Y. Keung, and T. C. Yuan, Phys. Rev. D **43**, 14 (1991); R. G. Leigh, S. Paban, and R.-M. Xu, Nucl. Phys. **B352**, 45 (1991). Multiple Higgs doublets are also important in the context of low-energy supersymmetry; for example, see H. Haber and G. Kane, Phys. Rep. **117**, 75 (1985).

[10] S. K. Lamoreaux, J. P. Jacobs, B. R. Heckel, F. J. Raab, and N. Fortson, Phys. Rev. Lett. **59**, 2275 (1987); S. A. Murthy, D. Krause, Jr., Z. L. Li, and L. R. Hunter, *ibid.* **63**, 965 (1989); D. Cho, K. Sangster, and E. A. Hinds, *ibid.* **63**, 2559 (1989); K. Abdullah, C. Carlberg, E. D. Commins, H. Gould, and S. B. Ross, *ibid.* **65**, 2347 (1990).

[11] E. E. Salpeter, Phys. Rev. **112**, 1642 (1958).

[12] P. G. H. Sandars, J. Phys. B **1**, 511 (1968).

[13] L. I. Schiff, Phys. Rev. **132**, 2194 (1963).

[14] P. G. H. Sandars, Phys. Lett. **14**, 194 (1965).

[15] S. M. Barr, Phys. Rev. D **45**, 4148 (1992).

[16] S. M. Barr, Phys. Rev. Lett. **68**, 1822 (1992).

[17] E. N. Fortson, in *Atomic Physics 10*, edited by H. Narumi and I. Shimamura (Elsevier Science, Amsterdam, 1987); E. N. Fortson (private communications).

[18] For the EDM of the Cs atom due to scalar interaction see C. Bouchiat, Phys. Lett. **57B**, 284 (1975); E. P. Venugopal, M. S. thesis, Utah State University, 1990. For Xe and TlF, calculations of EDMs due to both scalar and tensor interactions are reported in E. A. Hinds, C. E. Loving, and P. G. H. Sandars, Phys. Lett. **62B**, 97 (1975).

[19] W. R. Johnson, D. S. Guo, M. Idrees, and J. Sapirstein, Phys. Rev. A **32**, 2093 (1985).

[20] W. R. Johnson, D. S. Guo, M. Idrees, and J. Sapirstein, Phys. Rev. A **34**, 1043 (1986).

[21] J. Andriessen, Technische Universiteit Internal Report, Delft, The Netherlands, 1988 (unpublished); J. Andriessen, H. Postma, A. M. van den Brink, and T. P. Das, Phys. Rev. A **45**, 1389 (1992); also see E. P. Venugopal, Ref. [18].

[22] J. P. Desclaux, in *Relativistic Quantum Electrodynamic and Weak Interaction Effects in Atoms*, edited by W. R. Johnson *et al.* (American Institute of Physics, New York, 1989), p. 265.

[23] K. G. Dyall, I. P. Grant, C. T. Johnson, F. A. Parpia, and E. P. Plummer, Comput. Phys. Commun. **55**, 425 (1989).

[24] K. A. Brueckner, Phys. Rev. **100**, 35 (1955).

[25] A. C. Hartley, E. Lindroth, and A. M. Martensson-Pendrill, J. Phys. B **23**, 3417 (1990), and references therein.

[26] B. P. Das, W. R. Johnson, and M. Idrees (unpublished).

[27] P. G. H. Sandars, J. Phys. B **10**, 2983 (1977).

[28] P. G. H. Sandars, Phys. Lett. **22**, 290 (1966), and references therein.

[29] F. Coester, Nucl. Phys. **7**, 421 (1958); F. Coester and H. Kummel, *ibid.* **17**, 477 (1960); H. J. Monkhorst, Int. J. Quantum Chem. Symp. **11**, 421 (1977).

[30] Alok Shukla, B. P. Das, and D. Mukherjee, Phys. Rev. A (to be published).

[31] This can be seen as an application of Koopmans's theorem to double excitations. However, Koopmans's theorem is valid only for single excitations. Therefore, we term it as a crude approximation meant only for examining the relationship between perturbative and variational approaches. For Koopmans's theorem see T. Koopmans, Physica **1**, 104 (1933).